PROCEEDINGS OF SPIE

SPIEDigitalLibrary.org/conference-proceedings-of-spie

Carbon nanotubes thin filters for x-ray detectors in space

Marco Barbera, Ugo Lo Cicero, Luisa Sciortino, Michela Todaro, Elena Puccio, et al.

Marco Barbera, Ugo Lo Cicero, Luisa Sciortino, Michela Todaro, Elena Puccio, Fabio D'Anca, Nicola Montinaro, Salvatore Varisco, Pekka T. Törmä, Lauri Riuttanen, Ilkka Varjos, Bjorn Mikladal, Elena Magnano, Igor Pis, Christian Gollwitzer, Evelyn Handick, Michael Krumrey, Christian Laubis, "Carbon nanotubes thin filters for x-ray detectors in space," Proc. SPIE 12181, Space Telescopes and Instrumentation 2022: Ultraviolet to Gamma Ray, 121814H (31 August 2022); doi: 10.1117/12.2631516

SPIE.

Event: SPIE Astronomical Telescopes + Instrumentation, 2022, Montréal, Québec, Canada

Carbon NanoTubes thin filters for X-ray detectors in space

Marco Barbera*[a,b], Ugo Lo Cicero[b,a], Luisa Sciortino[a,b], Michela Todaro[a,b], Elena Puccio[a,b], Fabio D'Anca[b,a], Nicola Montinaro[c,b,d], Salvatore Varisco[b], Pekka T. Törmä[e], Lauri Riuttanen[e], Ilkka Varjos[f], Bjorn Mikladal[f], Elena Magnano[g,h], Igor Pis[g], Christian Gollwitzer[i], Evelyn Handick[i], Michael Krumrey[i], Christian Laubis[i]

[a]Dipartimento di Fisica e Chimica E. Segrè - Università degli Studi di Palermo (Italy); [b]Osservatorio Astronomico di Palermo - Istituto Nazionale di Astrofisica (Italy); [c]Département d'astronomie - Université de Genève (Switzerland); [d]Dipartimento di Ingegneria - Università degli Studi di Palermo (Italy); [e]Ametek Finland Ltd (Finland); [f]Canatu Oy (Finland); [g]Istituto Officina del Materiali - Consiglio Nazionale delle Ricerche (Italy); [h]Department of Physics, University of Johannesburg (South Africa); [i]Physikalisch-Technische Bundesanstalt (Germany)

ABSTRACT

In this paper, we present the first results from an investigation performed on nanometric thin pellicles based on carbon nanotubes (CNT) of potential interest for manufacturing large area optical blocking filters to protect soft X-ray detectors in astrophysics space missions. In order to evaluate the effective capability of such materials to block UV/VIS/IR radiation, while being highly transparent in the soft X-rays and strong enough to withstand the severe launch stresses, we have performed a suite of characterization measurements. These include: UV/VIS/IR and X-ray absorption spectroscopy, X-ray Photoelectron Spectroscopy and Scanning Electron Microscopy on bare and Al coated small self-standing pellicles; static mechanical tests on small freestanding samples.

Keywords: X-ray detectors for astrophysics, optical blocking filters, CNT, synchrotron, absorption spectroscopy, X-ray photoelectron spectroscopy, mechanical tests.

1. INTRODUCTION

Soft X-ray detectors for high-energy astrophysics presently used in space (e.g. on Chandra [1][2], XMM [3][4], e-Rosita [5]) or planned for future missions (e.g. on Athena [6][7], XRISM [8], eXTP [9]), including microcalorimeters and solid state detectors, are sensitive to photons outside the energy range of interest. Out-of-band radiation typically deteriorates the energy resolution, shifts the energy scale or increases the background noise thus significantly compromising the detector performance. Thin filters, highly transparent to X-rays, are thus needed in front of such detectors to fully exploit their high sensitivity.

Optical blocking filters, used in previous high-energy space missions, consist of a thin continuous 2D polymeric film, with thickness ranging from few tens to hundreds of nanometers, typically coated with a light metal which is very efficient in reflecting VIS/IR radiation (see the review paper [10]).
Within a Technology Research Program (TRP) funded by the European Space Agency (ESA) and leaded by AMETEK Finland Ltd, we are investigating large format very thin carbon nanotube (CNT) pellicles manufactured by Canatu OY Finland as a potential innovative material to fabricate large area thin filters to protect X-ray detectors in space. CNT

Space Telescopes and Instrumentation 2022: Ultraviolet to Gamma Ray, edited by Jan-Willem A. den Herder, Shouleh Nikzad, Kazuhiro Nakazawa, Proc. of SPIE Vol. 12181, 121814H · © 2022 SPIE · 0277-786X · doi: 10.1117/12.2631516

based filters can present interesting characteristics with respect to currently used thin polymeric films in terms of higher low-energy X-ray transparency, higher mechanical strength, and superior thermal conductance.

In terms of optical performance, CNTs have a low extinction coefficient and low flare at EUV and X-ray wavelengths with EUV transparencies up to 97% as well as high optical transparency [11][12]. These optical qualities, when combined with their high thermal resistance of up to 1500°C, chemical inertness, and high tolerance to pressure differentials make them ideal for performing in extreme environments. As a significant example, they have been proven to be very effective particle filters for photomasks used in EUV lithography [13][14]. Firstly, with its high transmittance, more light passes through the pellicle and reaches the wafer, increasing throughput. Secondly, due to its low flare, features can be printed with extreme precision without pattern distortion. Lastly, pellicles must meet stringent chemical, mechanical and thermal requirements to sustain such optical properties in a harsh EUV scanner environment. The pellicle has to thrive in a vacuum chamber and withstand extreme temperatures of approximately 600 to 1000ºC. Combined, these qualities ensure that EUV pellicles effectively protect the photomask from defects, thus enabling high yield and throughput in advanced semiconductor manufacturing.

Due to the above mentioned optical and mechanical properties, free-standing CNT pellicles also exhibit huge potentials as filters to protect X-ray detectors in space experiments. While manufacturing of large format pellicles with areas of hundreds of square centimeters has been proven [15], the main technology challenges for space applications are related to three topics: 1) maintaining the strength properties while reducing the thickness to provide high soft X-ray transmittance; 2) obtaining the required UV/VIS/IR attenuation; 3) prove stability in a space environment.

In order to provide high enough UV/VIS/IR attenuation and preserve an efficient soft X-ray transmittance, a thin highly reflective light metal layer, like aluminium, with thicknesses of few tens of nanometres must be deposited. However, CNT pellicles are not continuous 2D films, but meshes with a significant fraction of the area being empty (see Figure 1), thus, aluminium deposition may not be capable to fully bridge open gaps in the structure formed by the overlapping CNTs. To overcome this potential limitation, one option is to increase the surface density of the CNT meshes decreasing the air gaps on the surface. This needs to be done of course without losing the transmittance on the X-ray area.

The third technical challenge is related mainly to atomic oxygen which is present in Low Earth Orbits (LEO), less of a problem for high Earth or Lagrange point orbits like the one planned for Athena. It is already known that extremely thin and conformal atomic layer deposition (ALD) films such as AlO can be used to passivate structures against atomic oxygen. However, the relatively defect free C structure in the CNT offers a difficult growth surface for the inorganic molecules which easily results in a spotty/non-uniform coating. In order to try to solve this, pre-treatment is required which might be challenging when aluminium growth needs to be uniform across a wide area, extremely thin and pinhole free. The pre-treatments are also prone to damaging the CNT network so much that it weakens its basic properties such as mechanical strength which is required in the optical filter application. In the long run, multiwall tubes can be a good solution but it is not part of this investigation.
In this paper we report preliminary results from different characterization techniques used to evaluate the performance of CNT based filters. High spectral resolution X-ray transmittance measurements were used to verify compliance with requirements and to derive the areal densities of the involved elements (mainly aluminum and carbon), X-ray photoelectron spectroscopy (XPS) to estimate the amount of surface aluminium oxide, UV/VIS/IR spectroscopy to evaluate the out of band attenuation, and finally, bulge tests were performed to establish the resistance to static differential pressure. More characterization tests are being performed within the ESA RTP and will be reported elsewhere.

2. CNT BASED THIN FILTERS

CNTs are one-atom-thick carbon sheets rolled into tubes, single- or multi-walled, which can vary in diameter and in length. Engineered CNTs can be arranged in different configurations to form pellicles of different thicknesses and densities. Fully assembled filters, designed according to specific requirements, need three major fabrication steps: manufacturing of freestanding CNT pellicles, Al deposition, and assembly into the mechanical frame. Manufacturing shall be design oriented to a specific space application.

2.1 Requirements driving the filter design

The requirements, driving the design of the CNT based filters within this RTP, have been derived from the development program of the filters [19][20] for the X-ray Integral Field Unit (X-IFU) [7], one of the two focal plane X-ray detectors of the ESA large class high energy astrophysics space mission Athena [21]. Table 1 summarizes the requirements verified with the characterization tests reported in this paper.

Table 1. Main requirements driving the design of CNT based filters for X-ray detectors within the ESA funded RTP. Verification method is RD = Review of Design, T = Test.

Parameters	Specification	Notes	Verification
Dimension	Up to 130 mm clean aperture diameter		RD
Open area	> 97 %	To account for structural meshes	RD, T
X-ray Transmittance	> 73% @ 0.35 keV > 94% @ 1.0 keV > 97% @ 7.0 keV		RD, T
Visible/IR rejection	$< 5 \cdot 10^{-2}$ UV/Vis/NIR (200-2500 nm) $< 1 \cdot 10^{-3}$ MIR (2.5-25 μm) $< 1 \cdot 10^{-4}$ FIR (25-300 μm)	Driven by the photon shot noise on cryogenic microcalorimeters	RD, T
Static overpressure	2 mbar		T

2.2 CNT pellicles manufacturing

Canatu has developed unique manufacturing processes to create the most advanced CNTs for highly engineered solutions. Two key synthesis processes, namely Floating Catalyst Chemical Vapor Deposition (FC-CVD) and dry deposition, have allowed Canatu CNTs to outperform others.

Under the FC-CVD process, catalyst particles float downwards from top of the reactor with a carrier gas towards the membrane filter. CNTs grow on the catalyst particles before landing directly on the filter, forming the CNT film. After CNT film formed on the filter, it will be press transferred onto a substrate. Benefits of FC-CVD include being low-cost, readily scalable, and providing enhanced control of the CNT growth process.

Canatu has skipped the more traditional liquid dispersion step in favor of dry deposition. This effectively bypasses several detrimental steps used in liquid dispersion, such as ultrasonication which leads to defective CNTs that are less durable and more susceptible to bundling. Dry deposition thus results in cleaner, longer, and virtually defect-free CNTs. In principle, electrical conductivity and tensile strength increases with length and purity of the tubes, which leads to enhanced performance across various applications.

Furthermore, Canatu has exceptionally precise control over CNT synthesis, allowing for application-specific tailoring of CNT properties. Such tailoring variations include altering CNT orientation and network morphology, bundle size, synthesis chemistry, and coatings. For example, a common post-treatment for EUV pellicles is densification which ensures better adhesion of CNTs to the final frame material.

The method is closely based on the process described in [15],[16]. For the application here described SWCNTs are synthesized in bundles with lengths in the range of 5-10 μm and diameters in the range from few to few tens of nm. The thickness of the SWCNT films can be varied from a sub-monolayer[1] to a few micrometres depending on the collection time. After the transfer, the freestanding SWCNT film is densified with alcohol vapours, which reduces its roughness and changes the bundle structure of the network. Besides by densification parameters, bundling can also be controlled by the CVD synthesis parameters. With decreased bundling it is possible to get denser SWCNT network structure, which was found to be useful to improve deposition of a continuous aluminium layer. Figure 1 shows SEM images of CNT pellicles with different densities. More information on pellicle preparation and pellicle performance in various applications can be found in [17].

[1] When the amount of SWCNTs is insufficient to create a single continuous layer

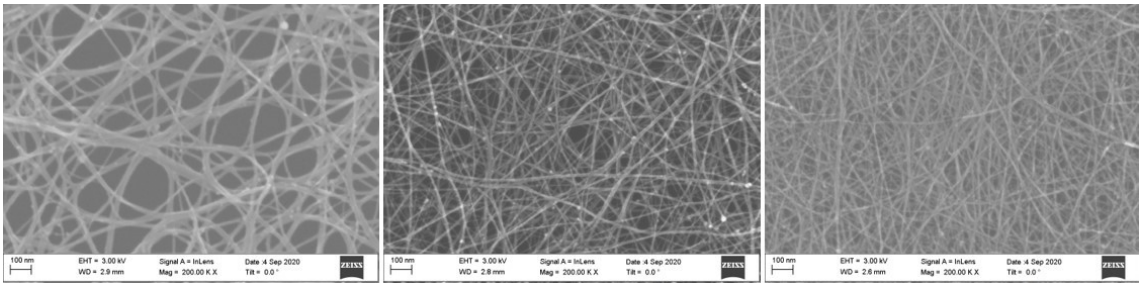

Figure 1. Canatu CNT networks with different densities i.e. bundle sizes. All sample networks contain an equal amount of CNTs. The network on the left has the lowest density i.e. largest bundle size. The one on the right has the same quantity of tubes spread more efficiently in smaller bundles, exhibiting the highest density i.e. smallest bundle size, whereas the central network falls between the two samples.

2.3 CNT pellicles coating and assembling

Al deposition onto CNT freestanding pellicles, SEM/optical inspections and frame assembly is performed at the premises of AMETEK Finland Ltd. The filter inner frame is the primary structure supporting the freestanding thin film, the outer frame provides mechanical stiffness, and serves as mechanical interface to mount the filter inside storage and shipping containers as well as onto the application system.

Deposition of Al is done with the MRC-900 series in-line sputtering. The system has few important features required in the filter fabrication. It offers exceptional flexibility with the geometry of the sample which can be basically anything up to 300 mm x 300 mm area and thickness up to 13 mm. The vacuum level and throughput are high due to the combination of separate load chamber and efficient cryo-pump of the main chamber. The large material target and scanning of the sample under target offer good uniformity. Al deposition parameters have been optimized by the fab supplier.

The Al deposition process for the CNT foils starts with pre-deposition bake. The CNT foils freestanding on Al alloy frames are first placed on the carrier plate, designed to avoid pressure differentials over the foil during pump and vent cycles, and baked at 120 °C for 15 minutes to reduce moisture in the CNT mesh. Then the plate is loaded in the load lock of the deposition tool and the chamber is slowly pumped down. The Al sputtering process is started after vacuum level of 5×10^{-7} mbar is reached. Figure 2 shows three different thicknesses of Al deposited on a CNT pellicle with smaller bundle size and higher density of bundles among those investigated in this activity (right panel in Figure 1).

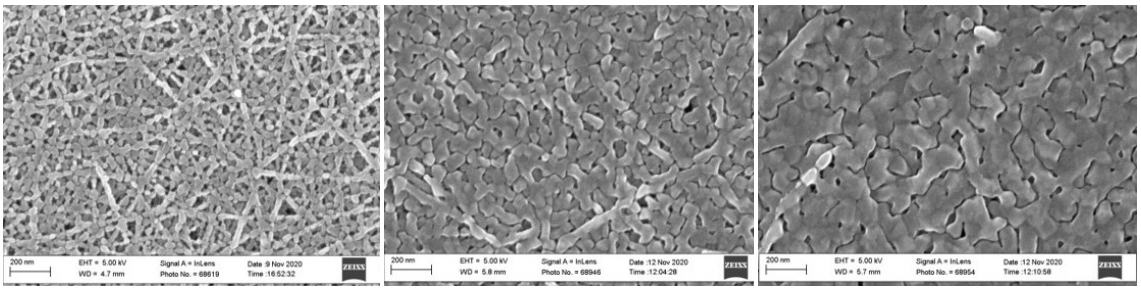

Figure 2. SEM images of three high density CNT networks manufactured by Canatu coated by AMETEK with an Al layer of different thicknesses, namely: 10 nm (left), 20 nm (center) and 30 nm (right).

After the Al deposition, the inner and outer frames are joined together with EPO-TEK H74F BI and EPO-TEK N20E adhesives. The first one is the primary adhesive and a droplet of the second one is used to create an electrical contact between the foil, the inner frame, and the outer frame. A gluing robot is used to place the structural epoxy with high

precision and exact volume inside the glue pocket on the outer frame so that it is located at the edges of the inner and outer frames. A small part of the pocket is left without epoxy for the drop of the conductive glue, which ensures the grounding the foil, inner frame, and outer frame to the same electric potential. The droplet of conductive glue is deposited manually on the outer frame. The assembled frames are placed on a graphite carrier and baked for 24 hours at 40 °C under a lid to cure the epoxy.

2.4 Tested Samples

The results reported in this paper are obtained from characterization measurements performed on small size CNT pellicle samples, bare or coated with aluminium, and with different densities mounted on circular aluminium frames with clear aperture diameters of 10 mm or 16 mm. CNT pellicles have been manufactured by Canatu Finland Oy with different bundle densities and an equivalent thickness tuned to be highly transparent in X-rays. Pre-treatment, aluminium coating, passivation and mounting on frames have been performed by AMETEK Finland Ltd. The outer diameter of these frames is 28.4 mm. The three different CNT network densities we investigated in this RTP, corresponding to different bundle sizes (the lower the density the larger the CNT bundle size), with nominally the same areal densities, are identified in the paper as low density (LD), medium density (MD), and high density (HD). The thickness of the aluminium is expressed in nanometers, a filter with a nickname HD0 is a high density bare CNT sample while HD30 is a high density CNT pellicle with 30 nm of aluminium deposited on one side.

Beside small size samples, large format filters have been manufactured mounted on supporting meshes according to the design of two of the thermal filters mounted inside the cryostat of the X-IFU on Athena, namely THF2 operating at 2 K (clear aperture diameter 56 mm) and THF300 which is the larger filter mounted on the outer main shell of the cryostat (clear aperture diameter 128 mm). Figure 3 shows pictures of the different types of manufactured CNT filter samples. From left to right: freestanding HD0 mounted on a circular frame with 10 mm clear aperture diameter, freestanding LD0 mounted on a circular frame with 16 mm clear aperture diameter, THF2 and THF300 with HD30 CNT pellicles supported by a Au plated BeCu alloy mesh with nearly 2% geometrical blocking factor.

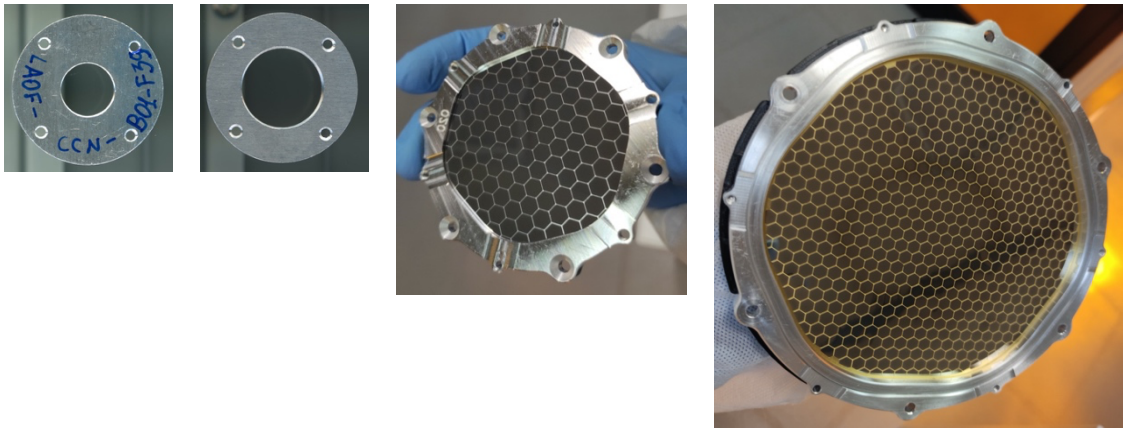

Figure 3. Pictures of four different CNT filter samples. The two samples on the left are HD0 mounted on TF110 and TF111 frames, respectively. The two filter samples on the right have been manufactured according to the design of the X-IFU thermal filters THF2 and THF300 on Athena. Pellicles are HD30 type and are supported by a Au plated BeCu alloy mesh with nearly 2% geometrical blocking factor.

A large number of samples have been investigated in the course of the RTP funded by ESA, here we report data and analysis only on a small subset of samples which are listed in each section describing a specific characterization technique. More extensive results, and additional characterizations will be presented elsewhere. The large format filter samples will undergo mainly environmental testing (thermo-vacuum, vibrations, differential pressure tests, micrometeorite impacts), and radio frequency attenuation tests. Results on this ongoing test campaigns will be reported elsewhere.

3. SPECTROSCOPIC CHARACTERIZATIONS

3.1 X-ray Transmittance

High spectral resolution X-ray transmittance measurements here reported were performed at the synchrotron beamline PTB-EUV/SX700 at BESSY II (Berlin, DE) [22] on small type samples to verify compliance with soft X-ray transmittance requirements, to derive the total amount of carbon, aluminium and aluminium oxide, and to search for contaminants (e.g. Fe). The energy range investigated at the beamline (50-1800 eV) includes edges of all elements expected to be present in the filters: Al L-edges @73 eV and @118 eV, C K-edge @282 eV, N K-edge @402 eV, O K-edge@532 eV, Fe L-edges @705 eV and @720 eV, and Al K-edge @1560 eV. Here we report only results from a subset of samples (see Table 2) measured in the test campaign conducted at BESSY in March 2021.

Table 2. List of small type samples characterized with X-ray Absorption Spectroscopy.

Sample name	Short name	CNT density	Al (nm)
LAOF-CCN-B02-F85	HD0	High	-
LAOF-CCN-B02-F57	MD0	Medium	-
LAOF-CCN-B02-F27	LD0	Low	-
LAOF-CCN-B02-F89	HD30	High	30
LAOF-CCN-B02-F38	MD30	Medium	30
LAOF-CCN-B02-F07	LD30	Low	30
LAOF-CCN-B02-F69	HD50	High	50
LAOF-CCN-B02-F41	MD50	Medium	50
LAOF-CCN-B02-F11	LD50	Low	50

Figure 4 shows the comparison between the transmittance plots of different density samples, either bare (left panel) or with an aluminium thickness of 30 nm (right panel). Inserts inside the main plot show details of the absorption edges. Data near the C K-edge were not acquired since in this energy range the signal is insufficient due to carbon contamination of the beamline optics.

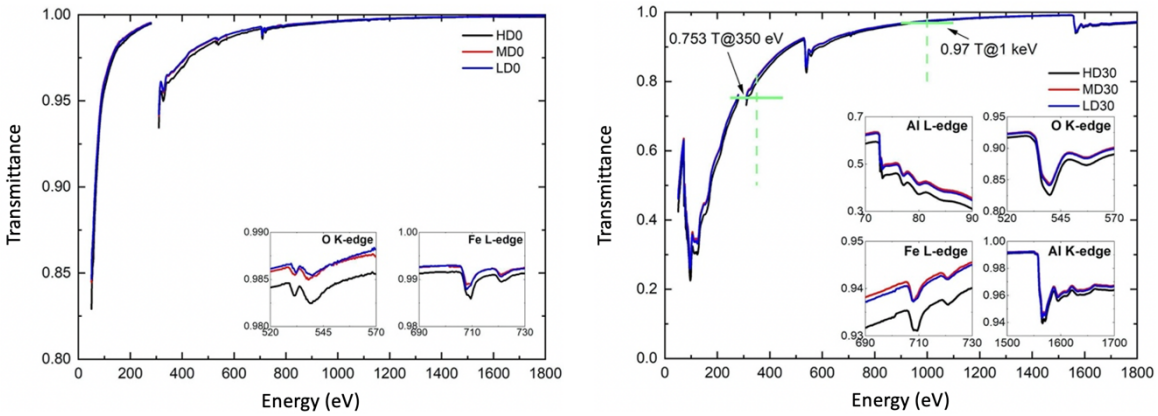

Figure 4. Comparison of HD/MD/LD with no Al (left) and with 30 nm of Al (right). The transmittance requirements at 350 eV and at 1 keV are reported in green.

By comparing the X-ray transmittance of CNT membranes coated with 30 nm of aluminium, and in particular the Al edges, it seems that the HD sample contains a slightly higher amount of Al. All samples are compliant with the X-ray transmittance requirements at 350 eV and at 1 keV reported in green.

In order to improve the IR attenuation of CNT networks (see also discussion in section 3.4) we have also investigated samples with different CNT densities and a thicker layer (50 nm) of aluminium (Figure 5 left panel). The thicker coating makes the transmittance slightly lower than the requirements at 350 eV and 1000 eV.

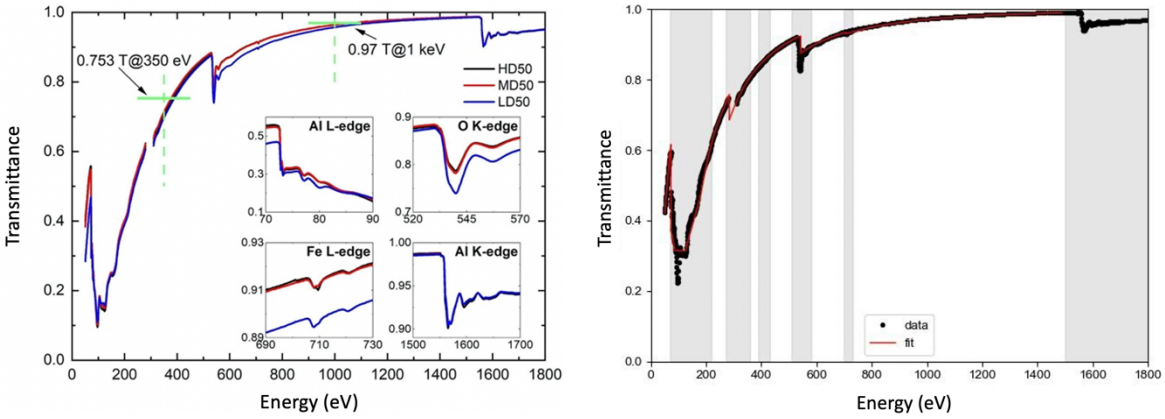

Figure 5. Comparison of HD/MD/LD with 50 nm Al (left). The transmittance requirements at 350 eV and at 1 keV are reported in green. The right panel is a plot of the X-ray transmittance data of HD30 CNT sample LAOF-CCN-B02-F89 (black points) together with the fitting model (red line). The data points inside the grey regions were excluded from the fit.

All the acquired data show a small but measurable amount of Fe as evident by the presence of the Fe $L_{2,3}$ absorption edge shown in the inset of the above data plots. Fe is one of the precursor for the growth of CNT and, in principle, it is not desirable on filters for X-ray detectors in space since Fe lines are of great astrophysical significance. To obtain a quantitative estimation of the amount of Fe as well as of the other elements present in the filters, the X-ray transmittance data were analyzed by using a transmission model to fit the experimental data outside the edge regions according to the modelling approach described in [23]. Figure 5 right panel is, as an example, the X-ray transmittance curve of the HD30 sample together with its best fitting curve. The best fit analysis gives the areal densities (ρt, ρ the density and t the thickness) of the elements composing the samples. In particular, the data of the bare CNT membranes were fitted by considering C, O and Fe, the data of the samples of CNT coated with aluminium were fitted by considering Al, C, O and Fe. The derived areal densities along with their 3σ statistical error are reported in Table 3.

Table 3. Areal densities of Al, C, O and Fe along with their 3σ statistical error derived from the best fit modelling.

		Areal density - ρx (10^{-7} g/cm^2)			
Sample name	**Short name**	**Al**	**C**	**O**	**Fe**
LAOF-CCN-B02-F85	HD0	-	12.4 (0.2)	2.60 (0.13)	0.4 (0.2)
LAOF-CCN-B02-F57	MD0	-	11.1 (0.2)	2.34 (0.12)	0.3 (0.2)
LAOF-CCN-B02-F27	LD0	-	10.9 (0.2)	2.33 (0.12)	0.4 (0.2)
LAOF-CCN-B02-F89	HD30	84.8 (0.5)	20.1 (0.5)	26.6 (0.5)	2.7 (0.6)
LAOF-CCN-B02-F07	MD30	79.4 (0.3)	17.8 (0.4)	23.5 (0.3)	2.2 (0.4)
LAOF-CCN-B02-F38	LD30	80.0 (0.4)	18.5 (0.4)	23.9 (0.3)	2.0 (0.4)
LAOF-CCN-B02-F69	HD50	145.3 (0.7)	24.1 (0.7)	26.3 (0.6)	2.9 (0.8)
LAOF-CCN-B02-F41	MD50	141.1 (0.7)	22.7 (0.7)	28.8 (0.5)	2.6 (0.8)
LAOF-CCN-B02-F11	LD50	146.6 (0.6)	26.8 (0.7)	40.6 (0.5)	2.6 (0.7)

Starting from the values reported in Table 3, we estimated the equivalent thickness of aluminium and of aluminium oxide coating the CNT membranes, as reported in Table 4. Al oxide thickness calculation starting from the O areal density in the sample minus that one of the bare CNT pellicle with the same density, whereas Al thickness from the Al areal density minus the Al contribution in the Al oxide. Total equivalent metallic Al thickness calculated assuming Al_2O_3 stoichiometry for aluminium oxide and densities of 2.7 g/cm^3 for metal Al and 3.3 g/cm^3 for Al_2O_3.

Table 4. Al and Al oxide thicknesses along with their 3σ statistical error derived from the best fit modelling of the transmittance curves.

Sample name	Short name	Al (nm)	Al_2O_3 (nm)
LAOF-CCN-B02-F89	HD30	21.4 (0.4)	15.4 (0.4)
LAOF-CCN-B02-F38	MD30	20.7 (0.3)	13.9 (0.3)
LAOF-CCN-B02-F07	LD30	20.6 (0.3)	13.6 (0.3)
LAOF-CCN-B02-F69	HD50	44.0 (0.5)	15.2 (0.4)
LAOF-CCN-B02-F41	MD50	41.2 (0.5)	17.1 (0.4)
LAOF-CCN-B02-F11	LD50	38.4 (0.5)	24.6 (0.4)

To conclude this section we show in Figure 6 a direct comparison between the X-ray transmittance measured on a high density CNT bare sample (HD0) with respect to a bare polyimide film 45 nm thick (left panel) and the same comparison between a CNT HD30 and a polyimide film 45 nm thick coated with 30 nm of Al (right panel). The HD0 is more transparent than the polyimide film in the very soft X-rays showing the high potentials of the CNT substrate for detectors which require high efficiency at very low energies. The HD30 sample presents a bit more aluminium than the coated polyimide film, as it is evident from the insets showing the Al L and K edges. Despite this, the CNT coated sample is more efficient at energies above the C K absorption edge.

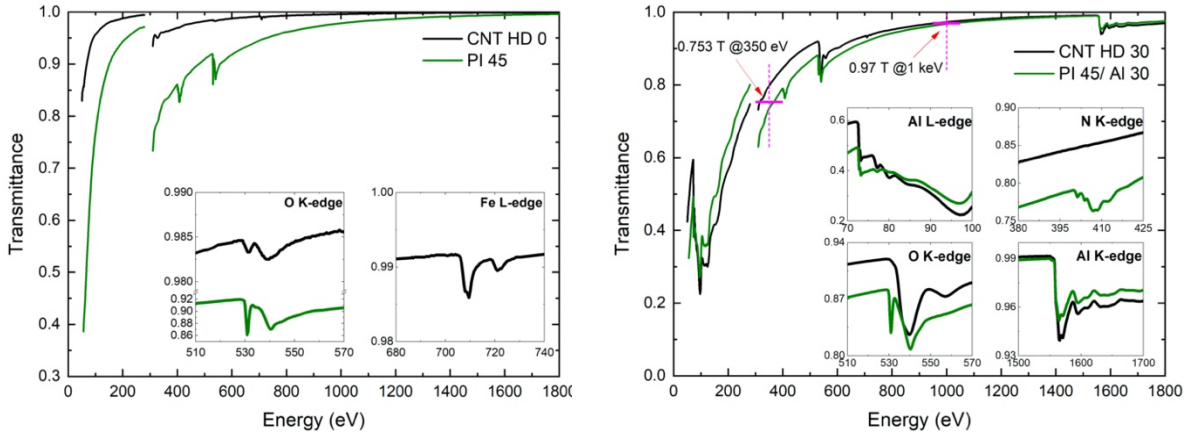

Figure 6. The left panel is a comparison between the X-ray transmittance of a CNT HD0 sample and a polyimide film 45 nm thick. The right panel compares the CNT and polyimide coated with 30 nm of aluminium.

3.2 X-ray Fluorescence Analysis

X-ray fluorescence (XRF) measurements were performed at the PTB four-crystal monochromator (FCM) beamline [24] at BESSY II using three different excitation energies 4 keV, 7.6 keV and 10 keV. The data here reported are only for the three different densities of bare CNT samples (first three lines in Table 2). The presence of Fe atoms is confirmed by the two detected lines at 6401 eV and 7069 eV ascribable to the K$\boldsymbol{\alpha}$ and K$\boldsymbol{\beta}$ fluorescence lines of iron (Figure 7, left panel). The Fe lines signal is extremely weak, though a quantitative analysis is ongoing, we have preliminary indications that the amount of iron present in the CNT networks is very likely not an issue for the use as filters in front of X-ray detectors for astrophysics. The spectrum obtained with incident energy of 4 keV (Figure 7, right panel) highlights the presence in traces of other low-Z chemical elements beside carbon, namely: oxygen, silicon, sulfur, and chlorine.

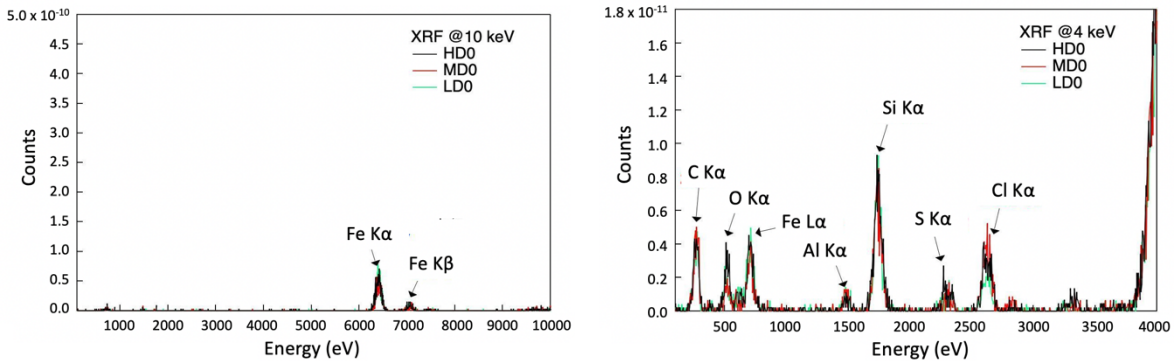

Figure 7. X-ray fluorescence spectra acquired with incident photon energy of 10 keV (left) and 4 keV (right)

3.3 X-ray Photoelectron Spectroscopy

XPS on aluminium coated CNT samples was performed at the BACH beamline at Elettra synchrotron with a hemispherical electron energy analyzer (Scienta R3000, VG Scienta) [25][26]. The full set of data and results will be discussed elsewhere while only preliminary findings are reported here on the different CNT density samples coated with 30 nm of aluminium investigated in September 2021 and listed in Table 5.

Table 5. List of small type samples characterized with X-ray Photoelectron Spectroscopy.

Sample name	Short name	CNT density	Al (nm)
LAOF-CCN-B01-F30	HD30	High	30
LAOF-CCN-B01-F19	MD30	Medium	30
LAOF-CCN-B01-F05	LD30	Low	30

We recorded Al 2p core-level spectra at four different kinetic energies of the outgoing electrons to probe different thicknesses of the sample, a technique known as “depth profiling”. In particular, the incident photon energies were set to obtain the kinetic energies of the outgoing electrons close to 720, 820, 920, and 1020 eV. Increasing the kinetic energy, photoelectrons probe deeper layers of the sample.

The Al 2p spectra are composed of two main signals: the larger one around 76 eV binding energy (BE) attributed to the Al3+ component (aluminium oxide) and a smaller one at about 73 eV assigned to Al0 component (metallic aluminium). In particular, the signal assigned to metallic Al is doublet due to the spin-orbit coupling. This doublet corresponds to the two possible states having distinguishable binding energies, attributed to $2p_{1/2}$ and $2p_{3/2}$ Al peaks (Figure 8 left panel). The binding energies were calibrated to Au $4f_{7/2}$ (84.0 eV) measured on a Au foil in electric contact with the samples.

To estimate the thickness d of the Al_2O_3 overlayer, we performed a linear fit of the aluminium oxide electron effective attenuation length, λo, according to Eq. 1 [26].

$$\lambda o = d/\sin\theta \ln((Nm*\lambda m*Io)/(No*\lambda o*Im)+1) \qquad (1)$$

where d is the thickness of the oxide layer, λo and λm are the electron effective attenuation length in the oxide and the metal, θ is the electron take-off angle with respect to the surface plane, No and Nm are the volume densities of the aluminium atoms in the oxide and the metal, and the Io and Im are the peak areas of the oxide and metal component of the Al 2p signal. The electron effective attenuation lengths were computed using the software released by the NIST Electron Effective-Attenuation-Length Database [29].

The data analysis was carried out using a convolution of gaussian and lorentzian components to fit the peaks. An example of peak analysis is reported in Figure 8 (left panel) for the HD30 sample. Metal and oxide peak areas are used as the input parameters to fit Eq.1 to derive the oxide thickness as the slope of the linear fit between λo and the inverse

of the logarithm of Eq. 1. The oxide thickness is found to be in the range of 5.4-5.8 nm. Figure 8 (right panel) shows an example of the fitting performed on the data of sample HD30. Considering that the surface topography of Al coated CNT is not planar (see Figure 2, right panel), the effective thickness calculated from Eq.1 can overestimate the oxide thickness and a correction factor smaller than 1 may be applied [27] (more details on the application of a proper topological factor will be discussed elsewhere).

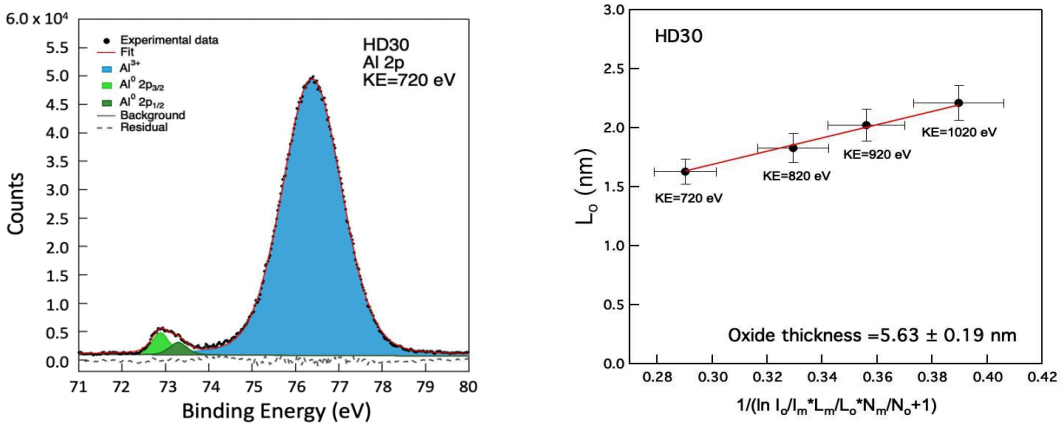

Figure 8. Left panel shows the XPS scan of the Al 2p peak at KE 720 eV of the HD30 sample. Experimental data (black circles), best fit (red solid line), $Al3^+$ 2p component (blue filled curve), Al0 $2p_{1/2}$ (dark green filled curve), Al0 $2p_{3/2}$ (light green filled curve), background (black solid line), and residual (black dashed line). The right panel is the linear fit performed on the data of the same sample HD30 to derive the oxide thickness according to equation 1.

The results of our analysis, for this subset of samples, are summarized in Table 6. The density of the CNT pellicles does not influence the thickness of the oxide. The amount of surface aluminium oxide, even correcting for surface topography, appears to be slightly larger than what measured on continuous polyimide membranes coated with aluminium (~ 3 nm) [30].

Table 6. Oxide thickness obtained from the linear fits using Eq. 1.

Sample name	Short name	Oxide thickness (nm)
LAOF-CCN-B01-F30	HD30	5.63 (0.19)
LAOF-CCN-B01-F19	MD30	5.66 (0.19)
LAOF-CCN-B01-05	LD30	5.55 (0.18)

3.4 UV/VIS/IR Spectroscopy

One of the key requirements of filters for X-ray detectors in space is the high level of attenuation of out-of-band radiation mainly in the UV/VIS/IR regions. Transmittance measurements, performed in this spectral region, are necessary to verify compliance to requirements, to constrain the transmission modeling and also to provide useful information such as: material thicknesses, metal oxidation, contamination, and aging.
The transmittance spectroscopy characterization of all investigated CNT filter samples was performed in UV-VIS-NIR bands using a double beam Perkin Elmer Lambda-1050 spectrophotometer, and in the MIR/FIR bands using a Perkin Elmer Spectrum 3 FT-IR spectrophotometer, both available in our laboratory at INAF-OAPA. Here we report results from a subset of samples listed in Table 7.
.

Table 7. List of small type samples characterized within UV/VIS/IR Spectroscopy.

Sample name	CNT density	Al (nm)	Passivation	Nickname
LAOF-CCN-B02-F86	High	-	-	HD0

LAOF-CCN-B02-F56	Medium	-	-	MD0
LAOF-CCN-B02-F25	Low	-	-	LD0
LAOF-CCN-B02-F63	High	30	native	HD30
LAOF-CCN-B02-F36	Medium	30	native	MD30
LAOF-CCN-B02-F06	Low	30	native	LD30
LAOF-CCN-B02-F68	High	50	native	HD50
LAOF-CCN-B02-F40	Medium	50	native	MD50
LAOF-CCN-B02-F09	Low	50	native	LD50
LAOF-CCN-B01-F36	High	30	AlO	HD30_ALD
LAOF-CCN-B01-F37	High	30	AlN	HD30_AlN

Figure 9, Figure 10, and Figure 11 show comparisons of measured transmittance for the three CNT densities (LD, MD, and HD) with different thicknesses of aluminium, namely: bare CNT samples without aluminium (Figure 9), samples with 30 nm of aluminium (Figure 10), and samples with 50 nm of aluminium (Figure 11). Figure 12 reports a comparison between high density CNT samples coated with 30 nm of aluminium without or with passivation either via ALD deposition or AlN. In all above plots a comparison is made with a polyimide film 45 nm thick bare or coated with 30 nm of aluminium (green line), since this material and design is the current baseline for the thermal filters of the X-IFU on Athena and thus a good reference to demonstrate the feasibility of CNT pellicle.

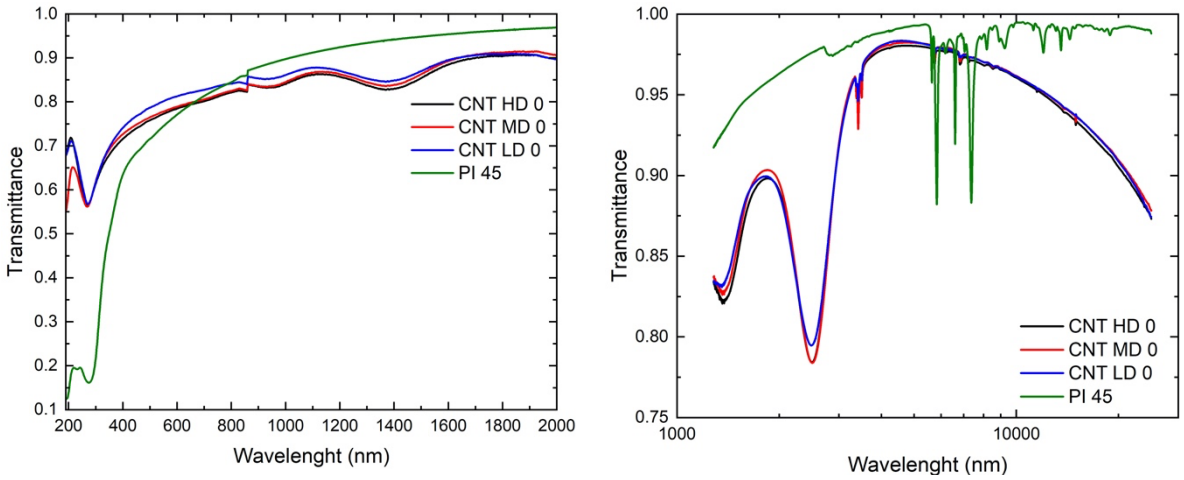

Figure 9. UV/VIS/NIR (left panel) and MIR (right panel) measured transmittance spectra for bare CNT membranes with the three different densities, namely: HD0 (black line), MD0 (blue line), and LD0 (red line).

All the naked membranes, as expected, show similar UV/Vis/IR transmittance since the carbon absorber atoms have nominally the same areal density and the same structure while only the density of CNTs is changed, in other words, the number of the absorbers, which are hit by the beam, is the same for all the CNT densities. The CNT is significantly more transparent than polyimide below ~400 nm, this is a disadvantage when it is needed to block the undesired bright UV emission of Astrophysical sources such as hot stars, on the other hand, it is an advantage for applications where the EUV is the target energy range of interest such as in space missions investigating the transition region and corona of the solar atmosphere.

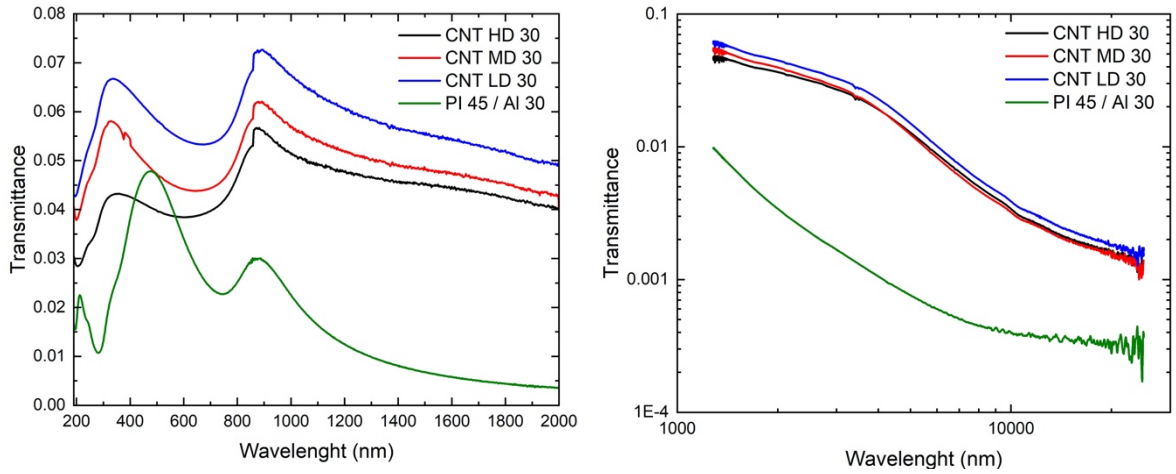

Figure 10. UV/VIS (left panel) and NIR (right panel) measured transmittance for CNT filter samples with about 30 nm of aluminium coating LAOF-CCN-B02-F63 HD30 (black line), LAOF-CCN-B02-F36 MD30 (blue line), and LAOF-CCN-B02-F06 LD30 (red line).

The transmittance of the HD30 CNT sample is $< 5 \cdot 10^{-2}$ in nearly all UV-Vis-NIR range thus compliant with the requirement for the thermal filters of the X-IFU on Athena. On the other hand the attenuation in the MIR range is not compliant and nearly an order of magnitude higher than PI45/Al30. Increasing the amount of aluminium to 50 nm (see Figure 11) allows to get the out of band attenuation of CNT filters within the requirements at the price of a lower transmittance in the soft X-rays. The HD50 filter sample outperform the PI45/Al30 in MIR attenuation, thus a smaller amount of aluminium could suffice to the purpose. An investigation is on-going to optimize the aluminium deposition parameters to improve the uniformity and thus increase the attenuation factor.

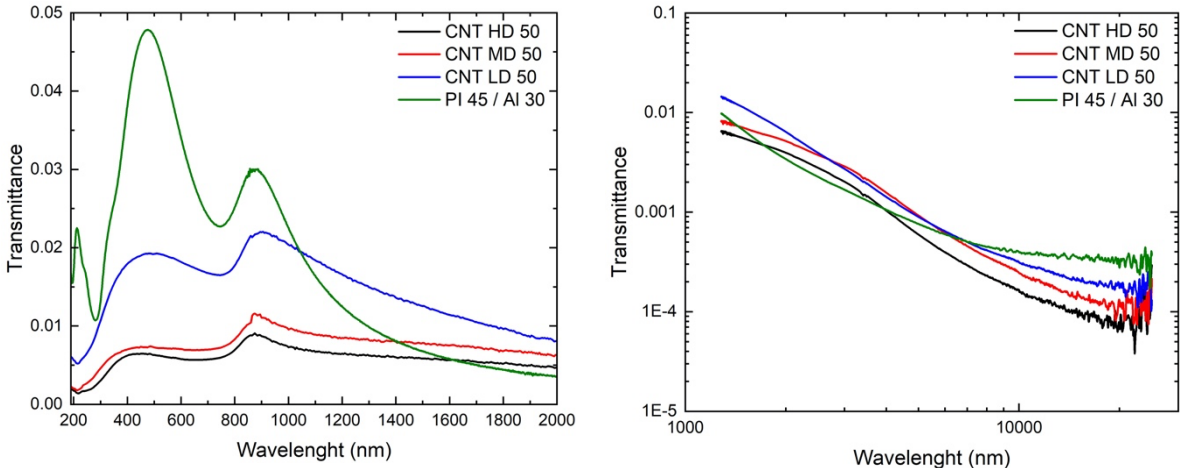

Figure 11. UV/VIS/NIR (left panel) and IR/MIR (right panel) measured transmittance for CNT filter samples with 50 nm nm of aluminium coating HD50 (black line), MD50 (blue line), and LD50 (red line). As a reference, the polyimide filter sample 45 nm thick coated with 30 nm of aluminium (green line).

Furthermore, high density CNT samples have been coated with 30 nm of aluminium and passivated with a surface layer of AlN or aluminium oxide deposited by ALD. Figure 12 shows the comparison of the passivated samples with respect to the HD30 with native passivation. The AlN passivated sample provides a higher attenuation and is thus considered as a promising solution to be further investigated.

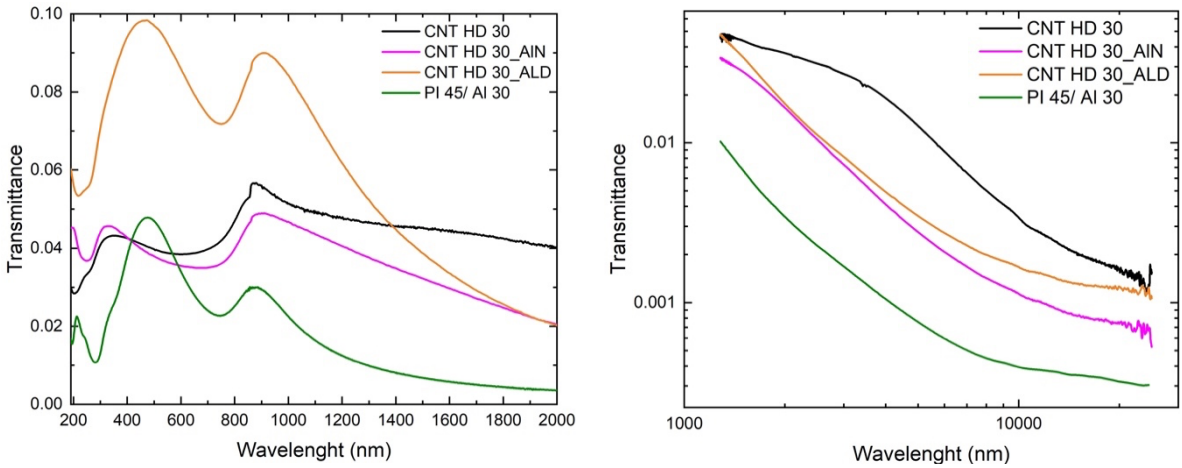

Figure 12. Comparison in UV/VIS/NIR (left panel) and IR/MIR (right panel) of measured transmittance for HD CNT samples coated with 30 nm of aluminium with native passivation (black), aluminium passivated with AlN (cyan), and aluminium passivated with ALD (orange). As a reference, the polyimide filter sample PI45/Al30 is also plotted (green line).

4. MECHANICAL CHARACTERIZATIONS

4.1 Static differential pressure

Filters developed for X-ray detectors in space shall withstand a moderate differential pressure occurring during vacuum/venting procedures. Static pressure load tests can be used to validate performances, measuring the membrane deflection under differential pressure load both in elastic regime and up to plastic deformation and failure. The experimental setup used for these tests at the XACT Facility of INAF-OAPA includes a computer controlled XY-stage, an optical confocal sensor, a leak tight sample holder, and a self-regulating pressuring system to apply and measure the differential pressure. The filter is mounted on a custom sample holder, sealed on the filter frame with an o-ring to allow the pressurization of the bottom face. The pressuring system allows to compensate for gas leaks, regulating the set pressure with an accuracy of 0.17 mbar. A more detailed description of the bulge test device set-up at INAF-OAPA is described in [31].

In order to study the elastic performance and possible onset of plasticization, the test sequence was divided in three consecutive load cycles, each one composed of a few pressure steps (see Figure 13)

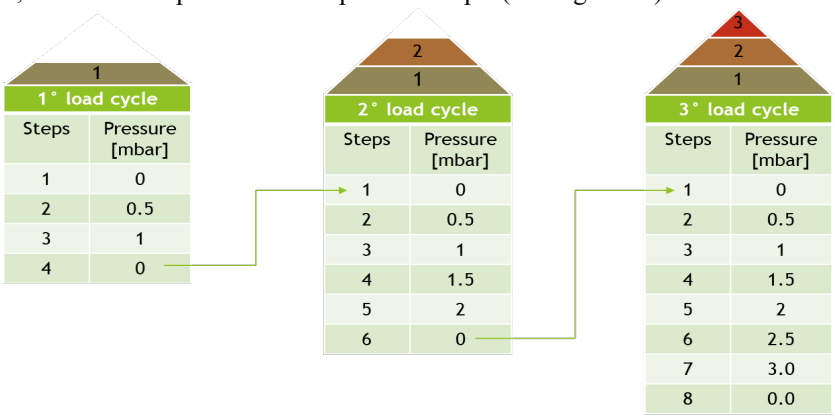

Figure 13. Sequence of load cycles used to study onset of the plasticization.

At each differential pressure step the deflected profile of the membrane is acquired, and the maximum deflection at the center of the bulge is extracted. Table 8 summarizes the test results, ordered from top to bottom according to time sequence, with a simple PASS/FAIL criteria. Notice that all the tested samples are mounted on TF111 frames with nearly 16 mm aperture diameter of the freestanding membrane. Considering that the actual X-IFU thermal filters will be supported by meshes with typical cell size < 5 mm, the maximum applied pressure on our samples corresponds to an applied pressure on cell size membranes more three times larger, thus well beyond the requirement (2 mbar).

Table 8. Summary of the PASS/FAIL results for all tested samples.

Sample Name	Nickname	Load cycles			
		1°	2°	3°	NOTE
LAOF-CCN-B02-F84	HD0	**PASS**	**PASS**	**PASS**	Tested twice
LAOF-CCN-B02-F86	HD0	**PASS**	**PASS**	**PASS**	
LAOF-CCN-B02-F55	MD0	**PASS**	**PASS**	**PASS**	Tested twice
LAOF-CCN-B02-F56	MD0	**PASS**	**PASS**	**PASS**	
LAOF-CCN-B02-F25	LD0	**PASS**	**PASS**	**N/A**	Too porous to exceed 2 mbar
LAOF-CCN-B02-F63	HD30	**PASS**	**PASS**	**PASS**	
LAOF-CCN-B02-F36	MD30	**PASS**	**PASS**	**FAIL**	Broken at about 3 mbar
LAOF-CCN-B02-F06	LD30	**PASS**	**PASS**	**N/A**	3° load not run for precaution
LAOF-CCN-B02-F61	HD20	**PASS**	**PASS**	**N/A**	3° load nor run for precaution
LAOF-CCN-B02-F31	MD20	**PASS**	**PASS**	**N/A**	3° load not run for precaution
LAOF-CCN-B02-F01	LD20	**PASS**	**FAIL**	**N/A**	Broken at 2 mbar
LAOF-CCN-B02-F09	LD50	**PASS**	**PASS**	**PASS**	
LAOF-CCN-B02-F40	MD50	**PASS**	**PASS**	**PASS**	
LAOF-CCN-B02-F68	HD50	**PASS**	**PASS**	**PASS**	

A first failure occurred on the MD30 sample at a pressure of about 3 mbar, after HD30 sample successfully passed the 3 mbar load test. As a consequence of this failure, in order to preserve the other samples for the subsequent optical characterizations, it was decided to lower the maximum pressure to 2 mbar, also on the third load cycle, on all the aluminized samples with thickness < 50 nm. In the prosecution of the campaign, a second failure involved the LD20 which broke once it reached the pressure of 2 mbar during the second load cycle.

A detailed analysis of the data collected on the full set of samples together with modelling of the mechanical performance of CNT bare and Al coated samples will be discussed elsewhere. In this paper we report only two preliminary results. Figure 14 (left panel) shows the loading curves of four MD samples: one bare (light blue) and three coated with 20 nm, 30 nm and 50 nm, respectively (orange, grey, and yellow). The plot clearly indicates that the coating increases the stiffness of the film since the max deflection is drastically reduced once the coating is applied. Figure 14 (right panel) shows the loading curves of different density CNT samples all coated with 50 nm of aluminium and indicated that stiffness of the CNT pellicles also increases with increasing density of the bundle networks.

As a global result of this test campaign, we can state that CNT bare membranes present a good resistance to moderate differential pressure, well above the requirement identified in the ESA RTP. It appears, however, that applying the aluminium coating may cause an embrittlement of the film and failure of some samples though still at pressure levels well above the requirements. Although the coating undoubtedly increases global stiffness, it is not clear if the stiffening effect is equally distributed or may cause local stress concentrations which can give birth to failures. Samples with less amount of aluminium (20 nm and 30 nm) as well as with lower densities are in fact more prone to develop discontinuity in the deposition thus leading to stress concentration and more chance of failure. Indeed, none of the many HD samples, bare and coated with aluminium, that have been tested presented any failure.

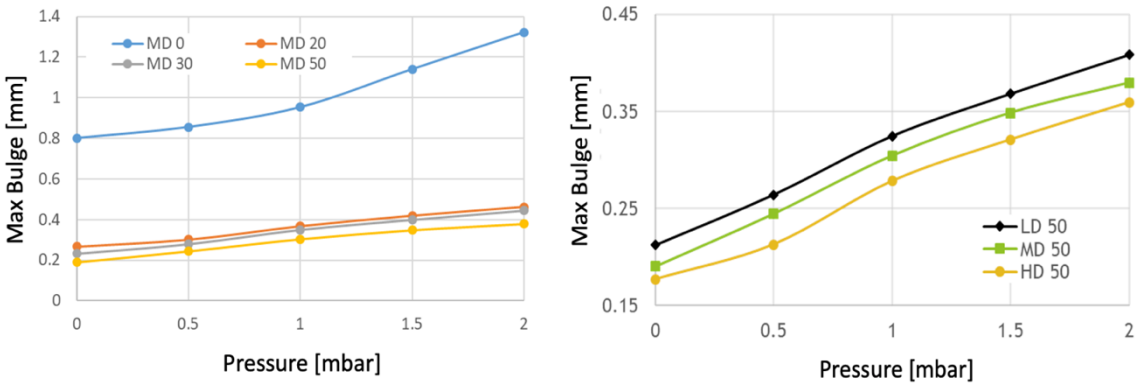

Figure 14. Max bulge deformation vs differential pressure plots for the MD samples with different thickness of coating (left panel, and for different CNT densities all coated with 50 nm of aluminium.

5. SUMMARY AND PERSPECTIVES

CNT pellicles originally developed for EUV microlithography present very interesting characteristics that make them an interesting material to manufacture large format very thin filters to protect X-ray detectors in space missions.

Under the support of the European Space Agency we are partner in a Research Technology Program leaded by Ametek Finland Ltd with the goal of designing, developing and characterising CNT based filters for space applications. The main driver of this RTP is presently to demonstrate the capability to manufacture filters like the ones currently designed for the Athena X-ray Integral Field Unit focal plane detector, which is under the responsibility of the UNIPA team, and try to raise the technology readiness level of this new technology to TRL5, according to ESA standards, in parallel with the technology readiness assessment activities of the baseline filters based on polyimide films.

In this paper we have reported some preliminary results of this RTP activity while more extensive results will be published in separate papers.

CNT pellicles are manufactured by Canatu Finland Oy, partner in the ESA funded RTP, with a proprietary recipe which is capable to deliver very large format (few hundreds of square centimeter), very thin (tens of nm), and uniform freestanding pellicles. The manufacturing process is versatile allowing to have control of the CNT bundle density and very good repeatability. Pellicles are attached to supporting metal meshes by means of intermolecular forces eventually promoted by chemical treatment of the mesh surface. Aluminium coating, final filter assembly and preliminary SEM and optical microscopy inspections is performed by Ametek. Design of the filters and full spectroscopic, mechanical and environmental characterization of the manufactured filters is performed under the responsibility of the UNIPA and INAF-OAPA team both in the laboratory in Palermo and at external facilities.

X-ray transmittance measurements performed in the PTB laboratory at the synchrotron radiation facility BESSY II on small samples of CNT filters, free standing on circular frames with 10 or 16 mm inner diameters, have shown that CNT based filters have very good X-ray transmittance, which could provide a measurable improvement in the X-IFU soft X-ray response with respect to polyimide/Al filters. Traces of Fe have been measured on the CNT pellicles by both X-ray transmittance and X-ray fluorescence measurements, however, the amount of Fe is so small that it is hardly detectable in the Fe K edge which is the energy region of astrophysical interest.

XPS measurements performed at the synchrotron beamline Bach at Elettra show that aluminium coated CNT pellicles present a native surface aluminium oxidation of about 5-6 nm which, even applying a correction factor for surface topography (~0.8 for cylindrical fibers), appears to be slightly larger than what measured on continuous polyimide membranes coated with aluminium (~ 3 nm).

The measured UV/VIS/IR and MIR attenuation of CNT/Al filters is lower than polyimide/Al, this is partially due to a more significant oxidation of the aluminium and to aluminium not fully bridging the network gaps between the CNT bundles. Different options are being investigated to improve the out of band rejection without the need to significantly increase the thickness of aluminium. One option is the use of surface passivation of aluminium either by a conformal oxide layer deposition by ALD or by a thin layer of AlN.

Differential pressure tests (bulge tests) have been performed on freestanding CNT pellicles of different densities, bare and coated with 20 nm, 30 nm, and 50 nm of Al mounted on circular frames with nearly 16 mm clear aperture diameter. All samples show a slight plasticization at pressures in the range 1-3 mbar. The rigidity of the samples increases with

the density of CNT bundles and with the thickness of the Al coating in the range 20-50 nm. Two samples have broken at a pressure larger than 2 mbar, both were coated with Al. Considering that the current requirement on differential pressure is 2 mbar and that filters will be supported by meshes with ~5 mm pitch, the current results show that CNT/Al samples are well compliant with respect to this requirement.
Large size filters have been manufactured mounted on BeCu alloy meshes with the design of two of the five filters stacked inside the cryostat of the Athena X-IFU detector, namely: THF2 operating at 2K with a 56 mm clear aperture diameter, and THF300 operating at a temperature above 300 K with a clear aperture diameter of 128 mm. Such filters will undergo a set of characterizations together with similar filters based on polyimide/Al to demonstrate the maturity of the technology, in particular, UV and IR mapping, X-ray mapping, differential pressure tests, vibration tests, thermo-vacuum. In addition, particles impact tests will be performed on a set of five CNT HD30 filters mounted in a stack to mimic the effects of micrometeorites impact in space on the focal plane of Athena, this activity will be funded by ESA within a Core Technology Program led by MPE (Garching, DE). Finally, a test campaign of atomic oxygen irradiation on small size samples with a dose a fraction of the lifetime of a space mission on a LEO will be performed at the ATOX facility of ESA in Estec (Noordwijk, NL).
Beside the potential use of CNT filters for Athena and/or future X-ray astrophysics space missions, this new technology has been recently identified as a promising solution to manufacture the telescope entrance filters and focal plane filters of the NASA MIDEX solar mission MUSE that will observe the solar transition region and corona in the EUV (10-30 nm) with fast high resolution spectroscopy and imaging. The Italian Space Agency will support the development of these filters for MUSE.

ACKNOWLEDGEMENTS

This investigation is funded by the European Space Agency RTP project “LAOF-CCN” (contract No. 4000120250/17/NL/BJ), and by the the European Union H2020 project “AHEAD2020” (contract. No. 871158). We acknowledge fruitful discussions and support by Alessandra Ciapponi and Marcos Bavdaz of ESA. We acknowledge Elettra Sincrotrone Trieste for providing access to its synchrotron radiation facilities and for financial support. E.M. and I.P. acknowledge funding from EUROFEL project (RoadMap Esfri).

REFERENCES

[1] Garmire, G. P., et al., “Advanced CCD imaging spectrometer (ACIS) instrument on the Chandra X-ray Observatory”, Proc. SPIE 4851 (2003), https://doi.org/10.1117/12.461599
[2] Zombeck, M. V., et al., “High-resolution camera (HRC) on the Advanced X-ray Astrophysics Facility (AXAF)”, Proc. SPIE 2518 (1995), https://doi.org/10.1117/12.218408
[3] Struder, L., et al., “The European Photon Imaging Camera on XMM-Newton: The pn-CCD camera”, A&A, 365, L18 (2001), https://doi.org/10.1051/0004-6361:20000066
[4] Turner, M. J. L., et al., “The European Photon Imaging Camera on XMM-Newton: The MOS cameras”, A&A 365, L27 (2001), https://doi.org/10.1051/0004-6361:20000087
[5] Meidinger, N., et al., “eROSITA camera array on the SRG satellite”, JATIS, 1, 014006 (2021), https://doi.org/10.1117/1.JATIS.7.2.025004
[6] Meidinger, N., et al., “Wide field imager instrument for the Advanced Telescope for High Energy Astrophysics”, JATIS, 1, 014006 (2014), https://doi.org/10.1117/1.JATIS.1.1.014006
[7] Pajot, F., et al., “The Athena X-ray Integral Field Unit (X-IFU)”. JLTP 193, 901–907 (2018), https://doi.org/10.1007/s10909-018-1904-5
[8] Ishisaki, Y., et al., “Status of Resolve instrument for X-ray astronomy recovery mission”, Proc. SPIE 1069924 (2018), https://doi.org/10.1117/12.2313440
[9] Zhang, S., et al., “The enhanced X-ray Timing and Polarimetry mission—eXTP“. Sci. China Phys. Mech. Astron. 62, 29502 (2019), https://doi.org/10.1007/s11433-018-9309-2
[10] Barbera, M., Lo Cicero U. and Sciortino L., “Filters for X-ray detectors on Space missions”, arXiv:2207.06781 [astro-ph.IM], https://doi.org/10.48550/arXiv.2207.06781

[11] Lee, J.U., et al., "Introducing the EUV CNT pellicle," Proc. SPIE 9985, (2016), https://doi.org/10.1117/12.2243019
[12] Pollentier, I., et al., "EUV scattering from CNT pellicles: measurement and control" Proc. SPIE 11609, (2021), https://doi.org/10.1117/12.2584718
[13] Pollentier, I., et al., "The EUV CNT pellicle: balancing material properties to optimize performance," Proc. SPIE 11323, (2020); https://doi.org/10.1117/12.2552357
[14] Timmermans, M.Y., et al., "Free-standing carbon nanotube films for extreme ultraviolet pellicle application," J.Micro/Nanolith. MEMS MOEMS 17(4), 043504 (2018), doi: 10.1117/1.JMM.17.4.043504
[15] Etula, J., et al., "Small scale, big impact: the world's thinnest and strongest free-standing carbon nanotube membrane," Proc. SPIE 11854 (2021), https://doi.org/10.1117/12.2599072
[16] Moisala, A., et al., "Single-walled carbon nanotube synthesis using ferrocene and iron pentacarbonyl in a laminar flow reactor", Chem. Eng. Sci., vol. 61, p. 4393–4402 (2006), https://doi.org/10.1016/j.ces.2006.02.020
[17] Nasibulin, A.G., et al., "Studies on Mechanism of Single-WalledCarbon Nanotube Formation" J. Nanosci. Nanotechnol., vol. 6, pp. 1233-1246 (2006), https://doi.org/10.1166/jnn.2006.340
[18] Nasibulin, A.G., et al., "Multifunctional freestanding single-walled carbon nanotube films", ACS Nano, 5, 4, 3214-3221 (2011), https://doi.org/10.1021/nn200338r
[19] Barbera, M., et al., "ATHENA X-IFU thermal filters development status toward the end of the instrument phase-A", Proc. SPIE 10699 (2018), https://doi.org/10.1117/12.2314450
[20] Barbera, M., et al., "Preliminary Mechanical Characterization of Thermal Filters for the X-IFU Instrument on Athena", J Low Temp Phys 193, 793–798 (2018), https://doi.org/10.1007/s10909-018-1942-z
[21] Barcons, X., et al., Journal of Physics Conference Series, 610, 012008 (2025), https://doi.org/10.1088/1742-6596/610/1/012008
[22] Scholze F., et.al., 'High-Accuracy EUV Metrology of PTB Using Synchrotron Radiation', Proc. SPIE 4344, 402-413 (2001), https://doi.org/10.1117/12.436766
[23] Puccio, E., et al., "Synchrotron X-ray transmission measurements and modeling of filters investigated for Athena", JATIS 6(3) 038003 (2020), https://doi.org/10.1117/1.JATIS.6.3.038003
[24] Krumrey M., and Ulm G., High-accuracy detector calibration at the PTB four-crystal monochromator beamline, Nucl. Instr. Meth. A 467-468, 1175-1178 (2001), https://doi.org/10.1016/S0168-9002(01)00598-8
[25] Zangrando, M., et al., "BACH, the beamline for advanced dichroic and scattering experiments at Elettra", Review of Scientific Instruments 72.2, 1313-1319 (2001), https://doi.org/10.1063/1.1334626
[26] Zangrando, M., et al., "Polarized high-brilliance and high-resolution soft x-ray source at Elettra: The performance of beamline BACH.", Review of scientific instruments 75.1, 31-36 (2004), https://doi.org/10.1063/1.1634355
[27] Shard, A. G., Wang J., and Spencer S. J., "XPS topofactors: determining overlayer thickness on particles and fibres." Surface and Interface Analysis: An International Journal devoted to the development and application of techniques for the analysis of surfaces, interfaces and thin films 41.7, 541-548 (2009), https://doi.org/10.1002/sia.3044
[28] Carlson, T.A., et al., "Basic assumptions and recent developments in quantitative XPS" Surf. Interface Anal., 4, 125–134 (1982), https://doi.org/10.1002/sia.740040402
[29] Powell, C.J., and Jablonski, A., NIST Electron Effective-Attenuation-Length Database - Version 1.3, National Institute of Standards and Technology, Gaithersburg, MD (2011), https://www.nist.gov/srd/nist-standard-reference-database-82
[30] Sciortino, L., et al., "Surface investigation and aluminium oxide estimation on test filters for the ATHENA X-IFU and WFI detectors", Proc. SPIE 9905 (2016), https://doi.org/10.1117/12.2232376
[31] Montinaro, N., et al., "Elastic characterization of nanometric plastic film for astrophysics application with an experimental-numerical method", Thin Solid Films under review (2022).

*marco.barbera@unipa.it; phone 39 091 233 613